3D Robotic Control of Micro-Scale Optical Swarms at an Interface

Nicholas Carlisle, *Graduate Student Member, IEEE*, Volker Nock, *Senior Member, IEEE*, Martin A.K. Williams, Catherine P. Whitby, Jack L.Y. Chen, and Ebubekir Avci

***Abstract*—Optical force-induced assembly is a promising yet scarcely explored approach for developing functional tools and objects at the microscale, with a wide range of potential applications. Our previous work was the first to investigate the manipulation of these assemblies in the XY plane. Here, we expand on these techniques by systematically exploring optical trap manipulation with the addition of Z-axis control. Manipulation of the Z-axis is referred to as axial displacement and is a viable approach for actively manipulating the assembly morphology. Experiments are conducted for the first time to explore and detail the response of the assembly during active 3D trap manipulation, informing the development of an autonomous control algorithm over the 2D area of the assembly during motion. This control presents techniques to increase assembly stability or alter the area of the assembly for tasks such as passing through constrictions. This work aims to develop the control techniques required to create a unique micromanufacturing approach inspired by the Kilobot thousand-robot swarm.**

***Index Terms*—Swarm robotics, micro/nano robots, automation at micro-nano scales.**

I. Introduction

SWARM technologies are set to play an increasingly important role in the future for many microrobotic applications due to their ability to complete tasks that individual microrobots can not [1], [2]. A key development currently being explored in literature is the ability to control microswarms as an entity to form functional microtools or objects. Applications for these functional swarms include forming tools for microsurgeries [3], [4], patterning structures for tissue engineering [5], [6], and manufacturing specific structures [7], [8]. However, the control approaches required to produce such technologies are currently limited.

Microrobotic swarms typically use an external energy source such as magnetic [9], acoustic [8], chemical [10], or optical [11] to induce self-assembling behaviour and control the swarm as an entity. Optical swarms are induced with a variety of approaches, including photocatalytic, photothermal, and optical force [12]. Optical force-induced assembly is driven by optical tweezers (OT) and is a promising approach for developing functional swarms that have yet to be comprehensively explored in literature.

OTs pass a laser through a high numerical aperture (NA) objective to form an optical trap. Forces acting on particles can be simplified to two forces: the scattering force pushing the particle along the propagation of the light, and the gradient force attracting the particle towards the focus of the laser. Successful particle trapping occurs in bulk solution when the gradient exceeds the scattering force. These forces are described under different regimes dependent on particle size, forces up to $\sim$ 10–20 pN per 100 mW can be achieved [13]. Similarly, holographic optical tweezers (HOT) use a spatial light modulator (SLM) to split and manipulate the laser before being focused through the objective. The SLM can produce multiple traps that can be simultaneously controlled with high spatial resolution within a 3D space.

Optical force-induced assemblies are formed when a trapped particle is moved to an interface, such as an air-liquid or glass-liquid interface; at the interface, the trapping laser scatters and propagates into the bulk, expanding optical potential, attracting and accumulating nearby particles and producing assemblies larger than the traps focal volume [11], [14], [15]. The forces required to trap at the interface are consistent with trapping in bulk; however, interactions with the interface help to immobilise particles, greatly reducing the required gradient force to trap the particle [11].

Current work on functionalising these assemblies is limited. Instead, available literature focuses on describing and tuning the assembly process by altering surface properties of the particles or interface [14], [15], [16]. Our previous work was the first to explore the active control of such assemblies [17], developing an algorithm to manipulate assemblies along the XY plane and to merge multiple assemblies at the air-liquid interface.

Received 25 November 2024; accepted 18 April 2025. Date of publication 8 May 2025; date of current version 27 May 2025. This article was recommended for publication by Associate Editor Z. Zhang and Editor X. Liu upon evaluation of the reviewers' comments. *(Corresponding author: Nicholas Carlisle.)*

Nicholas Carlisle, Volker Nock, and Ebubekir Avci are with the Department of Electrical and Computer Engineering, University of Canterbury, Christchurch 8041, New Zealand, and also with the MacDiarmid Institute for Advanced Materials and Nanotechnology, Wellington 6140, New Zealand (e-mail: nicholas.carlisle@pg.canterbury.ac.nz).

Martin A.K. Williams is with the MacDiarmid Institute for Advanced Materials and Nanotechnology, Wellington 6140, New Zealand.

Catherine P. Whitby is with the School of Fundamental Sciences, Massey University, Palmerston North 4442, New Zealand, and also with the MacDiarmid Institute for Advanced Materials and Nanotechnology, Wellington 6140, New Zealand.

Jack L.Y. Chen is with the School of Science, Auckland University of Technology, Auckland 1142, New Zealand, also with the Department of Biotechnology, Chemistry and Pharmaceutical Sciences, Universitá degli Studi di Siena, 53100 Siena SI, Italy, and also with the MacDiarmid Institute for Advanced Materials and Nanotechnology, Wellington 6140, New Zealand.

This article has supplementary downloadable material available at https://doi.org/10.1109/LRA.2025.3568304, provided by the authors.

Digital Object Identifier 10.1109/LRA.2025.3568304

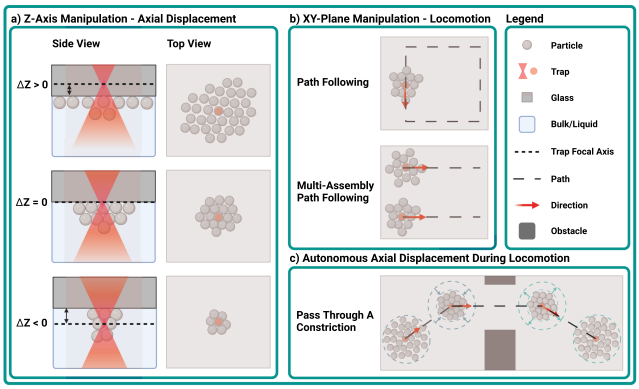

Fig. 1. Summary of the manipulation approaches explored in this study. (a) Z-axis manipulation explores the morphological response of the assembly when altering the distance between the HOT trap focal plane and the interface (ΔZ), referred to as axial displacement. (b) The XY-plane manipulation explores assembly stability during open-loop locomotion. c) The autonomous axial displacement experiment provides an example where an assembly is passed through a simulated constriction via PID control of axial displacement and open-loop locomotion.

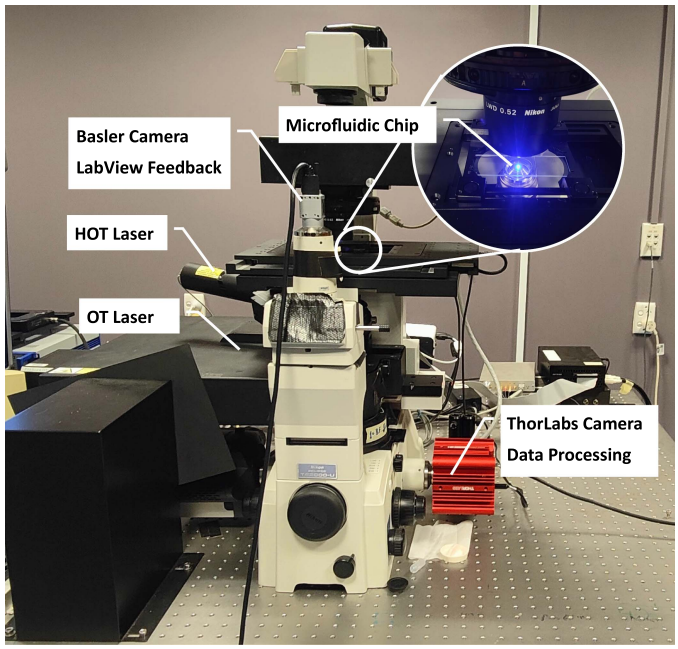

Fig. 2. Details of the optical system.

Optical force-induced assembly is a promising approach for developing a unique micromanufacturing approach inspired by the Kilobot thousand robot swarm [18], [19], where assemblies are produced, transported to, and bonded to a base assembly to form a larger complex structure. This study systematically investigates the assembly manipulation required to develop this micromanufacturing approach, culminating with autonomous control over the assembly morphology during motion, where future work will explore bonding approaches and develop the micromanufacturing algorithm.

Here, particle and assembly stability are investigated at the air-liquid and glass-liquid interfaces to optimise assembly control for autonomous experiments. Fig. 1 details three manipulation approaches explored in this study: 1a) axial displacement, 1b) locomotion, 1c) an example of an autonomous application. Axial displacement experiments describe the relationship between the manipulation of the Z-axis and the morphology of a stationary assembly. Locomotion experiments explore the capabilities of the system while following an open-loop path in the XY plane and characterise the role static axial displacement plays in altering stability during locomotion. Building on this, an exemplary autonomous application experiment was conducted that uses a PID controller to control the area of the assembly while passing through a simulated constriction. The main contributions of this work are as follows:

1) Exploration of dynamic control over axial displacement, developing an active control technique to manipulate the morphological structure of an assembly. To the best of our knowledge, previous investigations of axial displacement with optical force-induced assemblies have been limited to static control over an Au nanoparticle assembly [20].
2) Development of a PID algorithm for axial displacement, autonomously controlling assembly size while passing through a simulated constriction. This builds on our previous work and is the first example of autonomous manipulation of optical force-induced assemblies [17].

The structure of this letter is as follows. Section II details the system design, covering the OT system, microfluidic chip preparation, and the approach for experimental data processing. Section III compares the particle stability at the air-liquid and glass-liquid interfaces. Section IV explores the response of the assembly to HOT trap manipulation in 3D space and details autonomous control over the area of the assembly. Finally, Section V provides conclusions and future work for this study.

II. System Design

A. Optical System

Optical tweezers use a highly focused laser to trap dielectric particles. The change in momentum of photons during refraction exerts two forces on the particle: the gradient force is exerted along the spatial gradient of the light, pulling particles into the centre of the beam waist, and the scattering force is exerted along the direction of the light propagation. These two forces allow the particles to be precisely trapped in 3-dimensional space [13].

Fig. 2 shows the system used in this study, which consists of a 1030 nm OT laser and a 1064 nm HOT laser. This combination of lasers allows an assembly to be efficiently built with the OT trap, which is then replaced with a HOT trap for manipulation. The system uses two cameras, a feedback loop was implemented in LabVIEW with a CMOS camera (acA2040-90uc Basler, Germany), and data collection was achieved with an sCMOS camera (CC215MU ThorLabs, United States). A detailed description of this system can be found in Carlisle et al. [17].

All assemblies were built with the OT trap, running at 1 W for 60 seconds, producing a maximum force of approximately $\sim$ 100 pN. Manipulation is achieved with the HOT trap running at 2W; however, the power at the trap is significantly lower due

to the SLM splitting the laser. HOT trap strength depends on how the controlling hologram is formed.

B. Microfluidic Chip Preparation

The experimental colloidal solution contains carboxyl-coated polystyrene particles (Fluoresbrite YG Carboxylate Microspheres 1.00 μm Polysciences, USA) diluted with filtered Milli-Q water from 2.5% aqueous suspension to 0.01 vol% colloidal suspension.

All glassware used to fabricate the microfluidic chips (microscope slides and coverslips) was prepared as per Chang et al [14]. The glassware was immersed in a 5% solution of Hellmanex III (Sigma-Aldrich, USA), sonicated for 30 minutes, and left to soak overnight to negatively charge the glass surface, preventing electrostatic force interactions with the microparticles.

The glass-liquid interface consists of an imaging spacer with an internal diameter of 20 mm and a thickness of 0.12 mm (Grace Bio-Labs SecureSeal^{TM}imaging spacer Sigma-Aldrich, USA) on a 25 $\times$ 75 $\times$ 1 mm microscope slide, forming a well. 10 mL of the colloidal solution was placed into this well, then a 22 $\times$ 22 mm No.1 glass coverslip was used to seal the chip. The microfluidic chip is flipped so that the trapping laser can reach the top glass-liquid interface.

The air-liquid interface consists of an imaging spacer on a 22 $\times$ 60 mm No.1 glass coverslip forming a well. 10 mL of the colloidal solution was placed into this well, then a rubber O ring with a diameter of 20 mm and a 22 $\times$ 22 mm No.1 coverslip was placed on top to reduce evaporation and external interactions with the sample.

C. Image and Data Processing

Image processing is used to track assembly size and location and to form the system's feedback control loop. The particles used in this study are internally dyed to fluoresce with an excitation range of 441-486 nm, allowing fluorescence microscopy to be used rather than a more standard approach like bright-field microscopy.

Fluorescence microscopy uses a high-intensity light source to excite the fluorescent molecules, causing them to emit lower-energy light with a higher wavelength, which leaves a black background with a bright sample when filtered. Conversely, bright-field microscopy typically uses back-lighting to contrast a dark sample on a light background. The fluorescence approach greatly reduces the noise in the image by increasing contrast, eliminating artefacts, and reducing low-resolution blur from out-of-focus objects. Additionally, this technique allows for a simple thresholding algorithm to be used during image processing. Fig. 3 presents a visual comparison of images recorded using these two techniques and the effect on post-processing.

The image processing algorithms track the location (X, Y) and the 2D area of all detected fluorescing objects in the frame. The feedback loop identifies the assembly by cropping the incoming frame (250 x 250 pixels) around the known trap location, recording the data for the largest object. For collected data, a custom particle tracking algorithm in Matlab that tracks and separates objects between frames is used to identify the assembly.

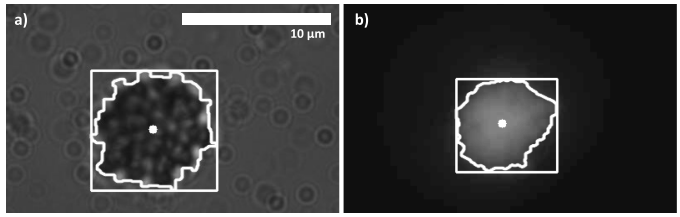

Fig. 3. Representative images illustrating the imaging techniques and resulting masking of the assembly post processing. (a) Bright-field microscopy. (b) Fluorescence microscopy.

III. Particle Stability At the Interface

Interfacial stability is an important factor in producing optical force-induced assemblies. In literature, these assemblies can be formed at the air-liquid or glass-liquid interfaces with similar dynamics [14], [21]. The stability of these interfaces are explored in two ways: tracking the motion of untrapped particles at the interface to explore vulnerability to external disturbances and counting particle ejections while building the assembly to study assembly volatility and efficiency.

A. Motion of Untrapped Particles

Particles are expected to exhibit Brownian motion at a stable interface [14]. Particle tracking was conducted over 10 seconds to identify particles at or near each interface and is presented in Fig. 4. Particles below the interface can temporarily drop from frame due to the Brownian motion along the Z-axis, when a particle is out of frame for an extended time or reemerges at a significant distance, the tracking algorithm classifies it as a separate object, indicated as distinct colours.

Particles at the air-liquid interface exhibit some Brownian motion with a consistent trend toward the bottom of the frame. This trend is consistent for particles at the interface but is less pronounced deeper in the bulk, indicating that this trend is likely due to external interactions such as air currents or gravitational interactions due to a non-flat interface (concave or convex). Additionally, a noticeable drop in interface height was present due to evaporation, requiring manual focal adjustment. Particles at the glass-liquid interface exhibit Brownian motion, indicating a more stable interface for particles.

B. Particle Ejections

Optical force-induced assemblies go through certain dynamics while forming [16]. When a particle is trapped at an interface, the laser scatters and propagates through the bulk, attracting nearby particles. Initially, the assembly forms a concentric circle (CC)-like structure. As particles continue to join the assembly, these collisions cause the particles in the assembly to fluctuate, triggering a structural rearrangement, leading to some particles being ejected from the assembly in a

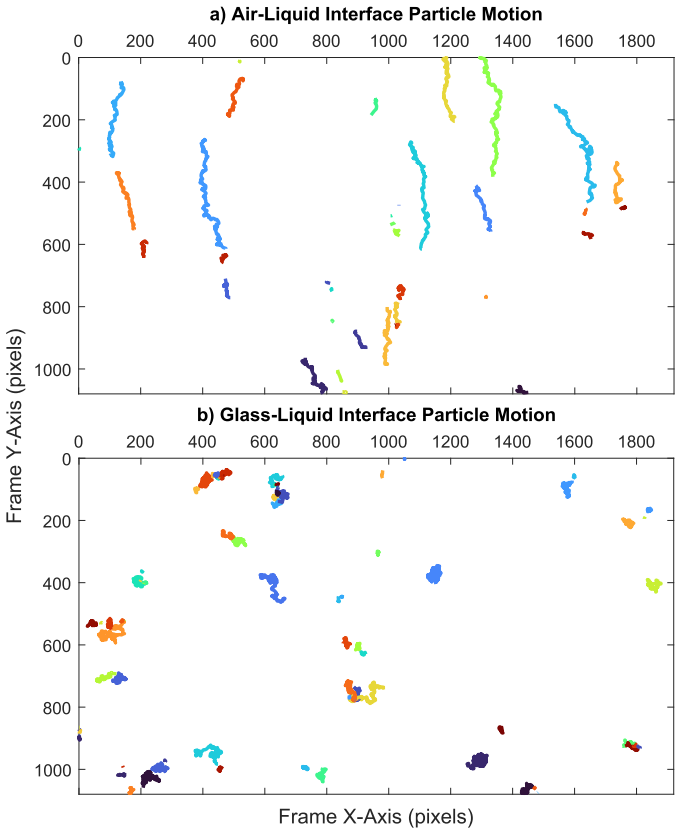

Fig. 4. Comparison of the movement of untrapped particles at air-liquid and glass-liquid interfaces. Each identified particle is indicated by a distinct colour. (a) At the air-liquid interface, particles exhibit a consistent drift toward the bottom of the frame, indicating an unstable interface. (b) At the glass-liquid interface, particles exhibit Brownian motion, indicating a stable interface.

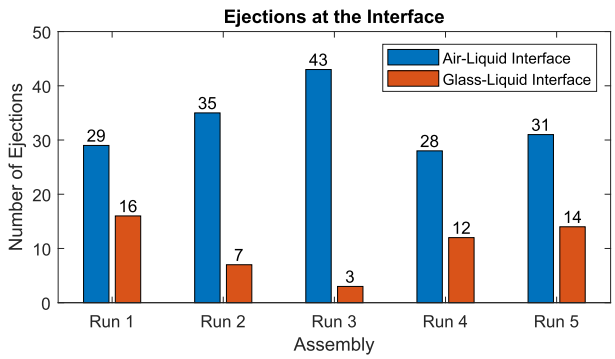

Fig. 5. Comparison of the number of ejections while building assemblies at the air-liquid and glass-liquid interface. The average number of ejections over 60 seconds is 33 for the air-liquid interface and 10 for the glass-liquid interface.

pistol-like fashion. These ejections allow the assembly to rearrange to a more stable hexagonal closely packed (HCP)-like structure.

Fig. 5 compares the quantity of ejection events at each interface, where the glass-liquid interface outperforms the air-liquid interface, averaging 10 ejections compared to 33 ejections over 60 seconds. The rigid nature of the glass-liquid interface mitigates vibrations, providing a stable packing of particles, efficiently scattering and propagating the trapping laser, and expanding the optical potential around the assembly [11]. Similarly to the tracking of untrapped particles, ejections occurring at the air-liquid interface tend to favour the same direction as the aforementioned drift. This indicates that factors such as the interfacial instability observed and localised heating causing inhomogeneous surface tension may also negatively impact the assembly stability at the air-liquid interface [11], [22].

IV. Assembly Manipulation Experiments

Controlled manipulation is the foundation for developing autonomous applications for optical force-induced assemblies. Our previous work [17] was the first to demonstrate HOT manipulation of assemblies in the XY plane, developing an approach to produce larger assemblies. Here, HOT assembly manipulation is explored in greater detail, focusing on trap manipulation within a 3-D space (XYZ) to understand the response and limitations of this technique. All experiments except static axial displacement are presented as the average response over five experiments, while the static experiment averages the area of a single assembly over 60 seconds.

A. Morphology Control via Axial Displacement

Huang et al proposed that photon momentum plays a role in shaping an assembly of gold nanoparticles [20]. They found that statically placing the trap focal plane above or below the interface influenced the structure formed by the particles. Manipulation of this axis, referred to as axial displacement is described in Fig. 1, where when $\Delta Z < 0$, the trap focal is in the bulk liquid, when $\Delta Z = 0$, the trap focal plane is in line with the interface, and when $\Delta Z > 0$, the trap focal plane is in the glass slide.

Axial displacement provides an interesting new possibility for controlling our optical force-induced assemblies. The RedTweezers software and SLA that control the HOT system can actively manipulate traps in 3-dimensional space without changing the focal plane of the microscope. Two experiments explore the response of our assembly during axial displacement: static and dynamic axial displacement.

1) Static Axial Displacement: The morphological response of the assembly was investigated in relation to its axial displacement. For this, an assembly is held for 60 seconds at axial displacements from -3 μm to +20 μm at 1 μm intervals. Due to particle ejections occurring near the lower limit, the experiment starts at the upper limit moving downward. The results of this experiment are shown in Fig. 6.

Axial displacement was demonstrated to be an important parameter for controlling assembly morphology. Positive displacement is associated with a perceived loosening of interparticle spacing, resulting in an increase in 2D area. Kamit et al explored the three-dimensional structure of optical force-induced assemblies using dual-objective lens microscopy. They inferred that under bright-field microscopy conditions, a darker core of the assembly indicates more particles below the surface, this same estimation can be used inversely for fluorescence microscopy, where a brighter core indicates a more 3D packing of particles [23]. We note that between axial displacements of

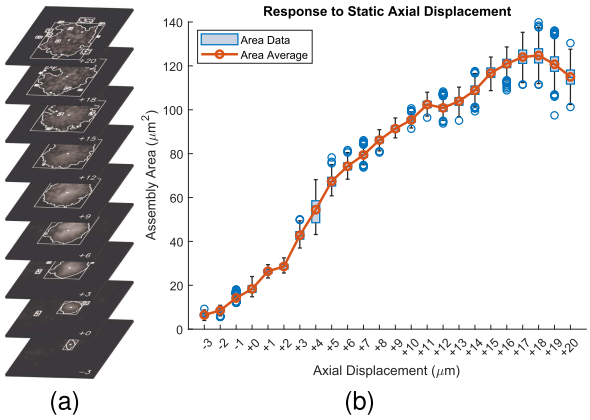

Fig. 6. Static axial displacement experiment shows the morphological response of the assembly by statically recording axial displacements ranging from +20 μm to −3 μm at 1 μm intervals. (a) Visual representation of the assembly at intervals throughout the experiment. (b) Data on the average area of the assembly throughout the experiment.

approximately +12 μm and +6 μm the fluorescence profile shifts from an even profile where individual particles are discernible to a profile with a bright centre, indicating that the assembly underwent a structural shift between a 2D to 3D structure (Fig. 6(a)). While descending, at axial displacements below +7 μm, particles are ejected from the assembly, increasing in rate towards the lower limit. The ejections indicate that assembly stability may be influenced by axial displacement.

Axial displacement limitations are inferred from this experiment. At negative axial displacements, the trapping dynamics revert to trapping singular particles in bulk, indicating a lower limit of +0 μm. The upper limit is based on the algorithms' performance. Above an axial displacement of +15 μm, the increased distance between particles and erratic particle motion within the assembly limits that algorithm's ability to identify the assembly as a single object as shown in Fig. 6(a). This also causes the increased fluctuation of the recorded assembly area presented in Fig. 6(b). Increasing the algorithms' performance at the higher axial displacement decreases performance for lower displacements, where ejected or nearby particles are mistakenly identified as part of the assembly.

2) Dynamic Axial Displacement: Fig. 7 presents the real-time response of the assembly to dynamic axial displacement. This experiment uses the abridged limitations of 0 μm to +15 μm, following a multi-step input function shown in the inset figure.

Dynamic axial displacement shows a slightly more unsettled response. As the assembly does not fully settle between steps, particle motion is more animated, and ejected particles are not given time to disperse from the assembly. This limits the accurate range of the algorithm to approximately +3 μm to +12 μm. These results indicate that gradual control of axial displacement will provide the best response for autonomous control.

B. Locomotion

Two experiments were conducted to explore the capabilities of the system during locomotion: open-loop path-following

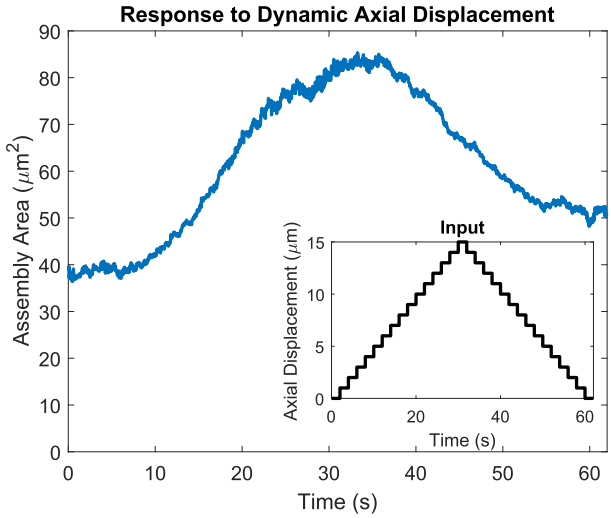

Fig. 7. Real-time response of the assembly to dynamic axial displacement. The inset figure shows the input signal, covering an axial displacement range of 0 μm to +15 μm.

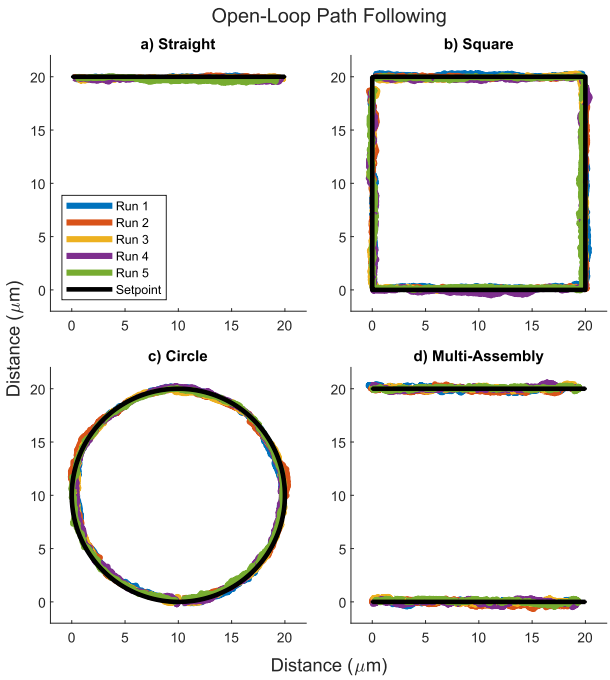

Fig. 8. Open-loop control of an assembly over predefined paths: (a) straight, (b) square, (c) circular, (d) multi-assembly straight path. The desired path is represented in black, while a different colour represents the paths taken by the assemblies in each run.

and 3-axis manipulation. A brief multi-assembly version of the locomotion experiments consisting of two assemblies moving synchronously in parallel is also conducted.

1) Path-Following: Locomotion is achieved by controlling the absolute position of the HOT trap relative to the feedback frame (X and Y pixel location). Fig. 8 presents three paths that cover the basic movements for any potential path (straight lines, sharp corners, and gradual curves): straight, square, and circular paths. These paths do not exceed 20 μm on either axis. The

TABLE I
ERRORS FROM THE OPEN-LOOP PATH-FOLLOWING EXPERIMENT

Experiment		Error (μm) Maximum	Mean	Standard Deviation
Path-Following	Straight	0.58	0.17	0.12
	Square	0.62	0.15	0.10
	Circle	0.68	0.19	0.13
Multi-Assembly	Top	0.88	0.16	0.13
	Bottom	0.91	0.17	0.14

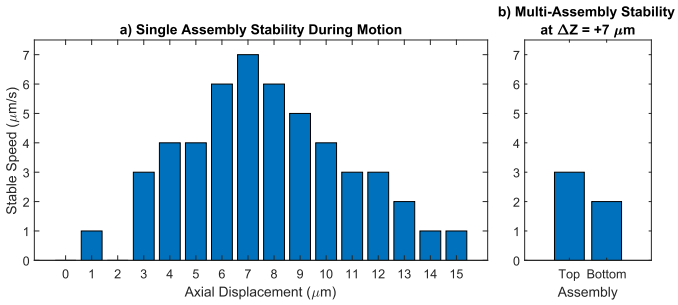

Fig. 9. Maximum stable speeds for each axial displacement. (a) Covers axial displacements from 0 μm to +15 μm for a single assembly. (b) Shows the multi-assembly experiment at an axial displacement of +7 μm.

multi-assembly experiment follows a straight path with a 20 μm distance between assemblies.

Table I summarises experimental errors. The maximum error is lower than 1 μm for each path, indicating high accuracy in open-loop control. During locomotion, a minor delay between trap movement and the assembly re-centering on the trap causes the assembly to cut corners during a change in direction to follow the shortest path. This accounts for the higher maximum errors in the square and circular paths and higher standard deviation errors for the circular path. The multi-assembly experiment incurred slightly higher errors comparatively, likely caused by the traps weakening when the laser is split.

2) 3-Axis Manipulation: The axial displacement experiments indicated that morphological control can increase assembly stability. Here, we explored how this translates to assemblies during locomotion. Assemblies travel a 20 μm straight path at axial displacements from 0 μm to +15 μm. With each pass, the speed increases by 1 μm/s until failure to find the stable range for each axial displacement. Failure for this experiment is calculated as a 20 % loss in assembly size compared to its original size during a single run. The results from this experiment are shown in Fig. 9(a) indicating a near-normal distribution.

The highest stability is found at an axial displacement of +7 μm, reaching 7 μm/s before failure. Due to this stability response and the 3D structural change observed in Section IV-A1 occurring in an overlapping axial displacement range, we propose that the increase in stability is related to the structural packing and interparticle distance of the assembly. Some factors limiting the stability of the assembly are the efficiency of the scattering pattern in maximising optical potential and the particle ejections caused by rearrangement of particles inside the assembly due to collisions with incoming particles [11], [16]. Therefore, the axial displacement of +7 μm may optimise lengthening the interparticle distances sufficiently, easing rearrangement without ejecting particles while maintaining an efficient structure for scattering and propagating the trapping laser. Complete eradication of ejections is unlikely without physically bonding the particles together. Irrespective of motion, the assembly is ever evolving, continually losing particles and absorbing new particles that enter the trap's region of effect. Therefore, we aim to maintain assembly size in lieu of the number of particles.

The 3-axis multi-assembly experiment shown in Fig. 9(b) was conducted at an axial displacement of +7 μm per previous results. Compared to the single assembly manipulation, splitting the laser to form multiple traps produces a significant drop in the stability of both assemblies, with the top assembly being stable at 3 μm/s and the bottom assembly at 2 μm/s. The difference in stability between the top and bottom assemblies indicates a potential difference in trap strength between the two HOT traps. While multi-assembly manipulation is possible, performance compared to single-assembly manipulation is limited.

C. Autonomous Axial Displacement

Autonomous control over the assembly is an important step for this technology. Here, we introduce the first stage in developing complete autonomous control. A PID controller is implemented to manipulate axial displacement, providing an effective and reliable approach for altering the morphology and 2D area of the assembly. Autonomous control over assembly morphology provides higher stability during experiments and allows the 2D area to be controlled for tasks such as passing through constrictions. Due to the results of the dynamic axial displacement experiments, the PID controller operates between +4 μm and +15 μm to reducing the likelihood of ejections due to changing axial displacement. The image processing algorithm is adjusted to ensure accuracy over this axial displacement range.

1) PID Controller Tuning: A PID controller was implemented and manually tuned in LabVIEW using the assembly area as the feedback variable. This controller updates at a frequency of 4 Hz and is tuned on a square wave alternating between a setpoint of 70 μm^2 and 90 μm^2 over a 40-second wavelength.

The optimum controller values were found at Kp = 0.1, Ki = 0.001, and Kd = 0.001, and the average response of the system is presented in Fig. 10. This response shows a rise time of 4.5 seconds, a fall time of 5 seconds, and a root mean squared error (RMSE) of 6.32. The system does not completely settle when the PID controller is running, instead, particle fluctuations cause consistent minor oscillations.

2) Simulated Constriction Algorithm: An exemplar experiment was devised to pass the assembly through a simulated constriction. For this experiment, the assembly follows a predefined path consisting of setpoints (X, Y, desired area). To stimulate passing through the constriction, the assembly starts at an area of 80 μm^2, reducing to 60 μm^2 to pass through the constriction, and then expands back to 80 μm^2 after the passage is complete. Fig. 11 presents the algorithm flow diagram.

The initialisation process that records the maximum and minimum area of the assembly is started when the user manually

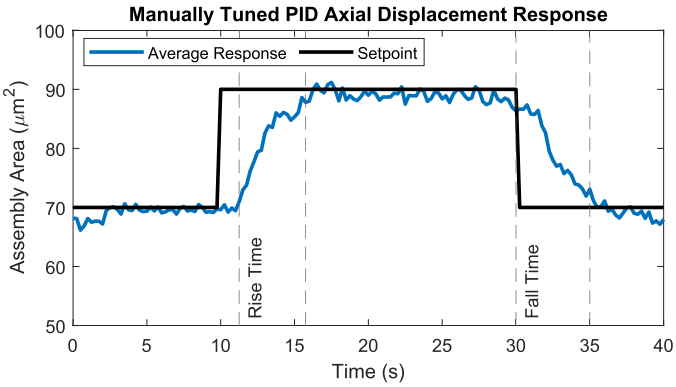

Fig. 10. PID controller response after manual tuning on a square wave alternating between 70 μm ^{2} and 90 μ m^2 setpoints.

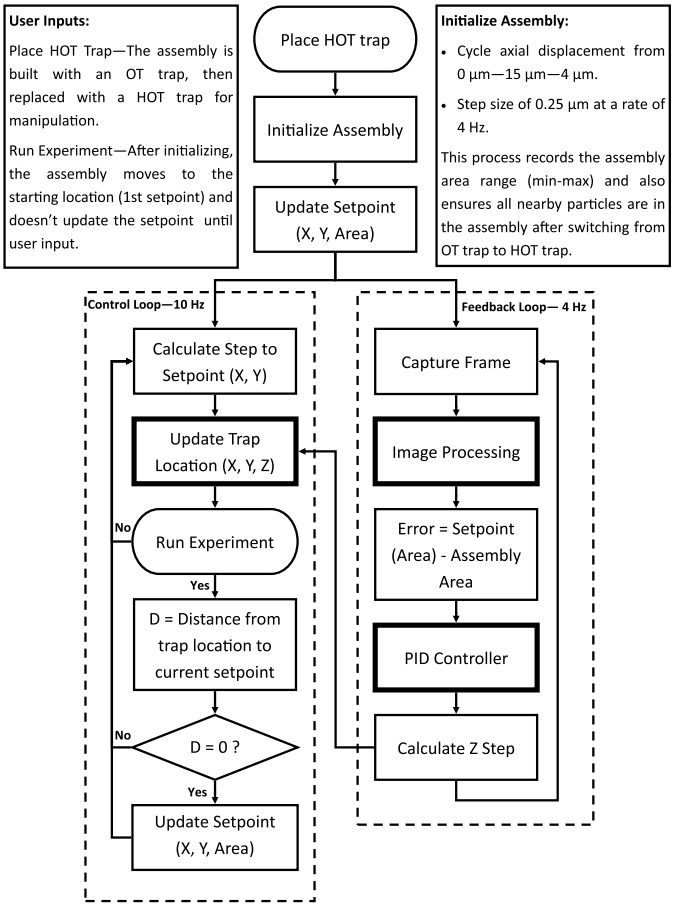

Fig. 11. Control flow diagram detailing algorithm for autonomous control over axial displacement while passing through a simulated constriction.

switches the trap from the OT system to the HOT system. Once initialisation is complete, the PID controller is started, moving the assembly to its starting location, where it waits for user input to run the experiment.

The algorithm consists of two parallel while loops (control and feedback) running at different frame rates. The control loop works at a rate of 10 Hz, calculating the assembly path (X, Y), updating trap location (X, Y, Z), and deciding when to update

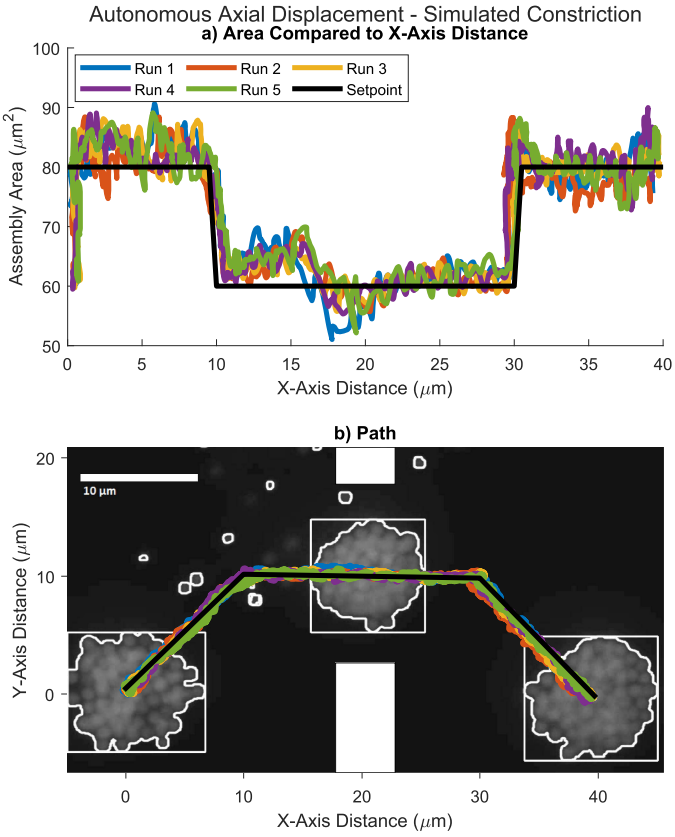

Fig. 12. Automation exemplar experiment, a PID controller is used to manipulate the 2D size of the assembly while passing through a simulated constriction. (a) Shows the response from the PID controller compared to the distance travelled along the X-axis. (b) Shows the path of the experiment overlaid on a visual representation of the experiment. The simulated constriction is indicated by the white objects.

the setpoint. The feedback loop works at a rate of 4 Hz, running the image processing and PID controller, calculating the new Z height, then passing it to the control loop. The difference in frame rate lets the feedback loop run in real-time while updating the trap location fast enough to produce smooth locomotion in the XY plane.

3) Simulated Constriction Experiment: During preliminary experiments, the combination of motion and a rapid drop in the assembly area caused significant ejections to occur. In response, a two-second pause in XY plane motion was added to the algorithm after the setpoint is updated, providing the assembly time to start changing area before the system accelerates at 1 μm/s ^{2} back to a maximum speed of 2 μ m/s. Fig. 12 presents the results from this experiment, with Fig. 12(a) plotting the assembly area against the distance travelled along the X-axis, and Fig. 12(b) showing the experimental path overlaid on a combined image of the experiment. The path was designed to change setpoints at 10 μm and 30 μm along the X-axis distance, allowing the assembly area to be plotted against motion rather than time.

While the pause in locomotion greatly reduces the severity of ejections, a small ejection event is still present when the assembly restarts movement through the constriction. This is seen in Fig. 12(a) as a slight increase in area followed by a

TABLE II
PID CONTROLLER PERFORMANCE COMPARING TUNED RESPONSE TO THE EXPERIMENTAL RESPONSE

PID Response	Rise Time (s)	Fall Time (s)	RMSE
Stationary Square Wave	4.5	5	6.32
Experiment Simulated Constriction	6.43	3.67	6.69

sharp drop. This ejection is deemed minor as it does not affect the overall performance of the assembly, expanding back to the original size.

Table II compares the experimental response to the tuned response for the PID controller. The increased rise time and the decreased fall time are consistent with our expectation of an assembly in motion. The increase in RMSE from 6.32 to 6.69 indicates a slight drop in performance. However, this is still deemed a good performance for this experiment.

The autonomous control demonstrated in this study completes the first stage of developing a unique micromanufacturing approach, showing the capabilities of the system towards creating functional tools for autonomous applications.

V. CONCLUSION

This letter explored the manipulation of optical force-induced assemblies by controlling the HOT trap in 3D space. Active manipulation of assembly morphology is presented for the first time, achieved through the dynamic manipulation of the Z-axis of a HOT trap. Culminating in an exemplary autonomous experiment that shrinks an assembly to pass through a simulated constriction, this experiment runs via open-loop locomotion and PID control of axial displacement. This work develops the control required to functionalise assemblies towards autonomous application, aiming to develop a unique micromanufacturing method. Future work towards this goal will focus on integrating a path-planning algorithm into the system and developing a bonding technique to mechanically set the particles and assemblies together to form a permanent structure.

REFERENCES

[1] L. Yang, J. Yu, S. Yang, B. Wang, B. J. Nelson, and L. Zhang, "A survey on swarm microrobotics," *IEEE Trans. Robot.*, vol. 38, no. 3, pp. 1531–1551, Jun. 2022.

[2] M. Dorigo, G. Theraulaz, and V. Trianni, "Reflections on the future of swarm robotics," *Sci. Robot.*, vol. 5, no. 49, 2020, Art. no. eabe4385.

[3] M. Luo et al., "Robotic swarm control for precise and on-demand embolization," in *Proc. 2020 IEEE Int. Conf. Robot. Automat.*, 2020, pp. 4470–4476.

[4] Q. Wang et al., "Reconfigurable magnetic microswarm for accelerating tPA-mediated thrombolysis under ultrasound imaging," *IEEE/ASME Trans. Mechatron.*, vol. 27, no. 4, pp. 2267–2277, Aug. 2022.

[5] D. R. Albrecht, G. H. Underhill, T. B. Wassermann, R. L. Sah, and S. N. Bhatia, "Probing the role of multicellular organization in three-dimensional microenvironments," *Nature Methods*, vol. 3, no. 5, pp. 369–375, 2006.

[6] J. P. Armstrong and M. M. Stevens, "Using remote fields for complex tissue engineering," *Trends Biotechnol.*, vol. 38, no. 3, pp. 254–263, 2020.

[7] D. Jin, J. Yu, K. Yuan, and L. Zhang, "Mimicking the structure and function of ant bridges in a reconfigurable microswarm for electronic applications," *ACS Nano*, vol. 13, no. 5, pp. 5999–6007, 2019.

[8] K. Melde, E. Choi, Z. Wu, S. Palagi, T. Qiu, and P. Fischer, "Acoustic fabrication via the assembly and fusion of particles," *Adv. Mater.*, vol. 30, no. 3, 2018, Art. no. 1704507.

[9] H. Xie et al., "Reconfigurable magnetic microrobot swarm: Multimode transformation, locomotion, and manipulation," *Sci. Robot.*, vol. 4, no. 28, 2019, Art. no. eaav8006.

[10] J. Palacci, S. Sacanna, A. P. Steinberg, D. J. Pine, and P. M. Chaikin, "Living crystals of light-activated colloidal surfers," *Science*, vol. 339, no. 6122, pp. 936–940, 2013.

[11] H. Masuhara and K.-i. Yuyama, "Optical force-induced chemistry at solution surfaces," *Annu. Rev. Phys. Chem.*, vol. 72, pp. 565–589, 2021.

[12] J. Law, J. Yu, W. Tang, Z. Gong, X. Wang, and Y. Sun, "Micro/nanorobotic swarms: From fundamentals to functionalities," *ACS nano*, vol. 17, no. 14, pp. 12971–12999, 2023.

[13] C. J. Bustamante, Y. R. Chemla, S. Liu, and M. D. Wang, "Optical tweezers in single-molecule biophysics," *Nature Rev. Methods Primers*, vol. 1, no. 1, 2021, Art. no. 25.

[14] Y.-C. Chang, R. Bresolí-Obach, T. Kudo, J. Hofkens, S. Toyouchi, and H. Masuhara, "The optical absorption force allows controlling colloidal assembly morphology at an interface," *Adv. Opt. Mater.*, vol. 10, no. 13, 2022, Art. no. 2200231.

[15] S. Pradhan, C. P. Whitby, M. A. Williams, J. L. Chen, and E. Avci, "Interfacial colloidal assembly guided by optical tweezers and tuned via surface charge," *J. Colloid Interface Sci.*, vol. 621, pp. 101–109, 2022.

[16] J.-S. Lu et al., "Optical force-induced dynamics of assembling, rearrangement, and three-dimensional pistol-like ejection of microparticles at the solution surface," *J. Phys. Chem. C*, vol. 124, no. 49, pp. 27107–27117, 2020.

[17] N. Carlisle, M. A. Williams, C. P. Whitby, V. Nock, J. L. Chen, and E. Avci, "Manipulation of optical force-induced micro-assemblies at the air-liquid interface," in *Proc. 2023 IEEE/RSJ Int. Conf. Intell. Robots Syst.*, 2023, pp. 2709–2714.

[18] M. Rubenstein and W.-M. Shen, "Automatic scalable size selection for the shape of a distributed robotic collective," in *Proc. 2010 IEEE/RSJ Int. Conf. Intell. Robots Syst.*, 2010, pp. 508–513.

[19] M. Rubenstein, A. Cornejo, and R. Nagpal, "Programmable self-assembly in a thousand-robot swarm," *Science*, vol. 345, no. 6198, pp. 795–799, 2014.

[20] C.-H. Huang, T. Kudo, T. Sugiyama, H. Masuhara, J. Hofkens, and R. Bresoli-Obach, "Photon momentum dictates the shape of swarming gold nanoparticles in optical trapping at an interface," *J. Phys. Chem. C*, vol. 125, no. 34, pp. 19013–19021, 2021.

[21] T. Kudo, S.-F. Wang, K.-i. Yuyama, and H. Masuhara, "Optical trapping-formed colloidal assembly with horns extended to the outside of a focus through light propagation," *Nano Lett.*, vol. 16, no. 5, pp. 3058–3062, 2016.

[22] S. Ito, T. Sugiyama, N. Toitani, G. Katayama, and H. Miyasaka, "Application of fluorescence correlation spectroscopy to the measurement of local temperature in solutions under optical trapping condition," *J. Phys. Chem. B*, vol. 111, no. 9, pp. 2365–2371, 2007.

[23] A. Kamit et al., "Unraveling the three-dimensional morphology and dynamics of the optically evolving polystyrene nanoparticle assembly using dual-objective lens microscopy," *J. Chin. Chem. Soc.*, vol. 69, no. 1, pp. 120–132, 2022.